Tunable Circular Dichroism Based on Graphene-Au Chiral Metasurface Structure

Gongli Xiao, Sitong Zhou, Hongyan Yang, Bing Wang, and Haiou Li

***Abstract*—In this study, we present a chiral metasurface structure based on graphene-Au elliptical hole arrays. Circular dichroism of up to 0.91 is achieved by varying the rotation angle of the elliptical hole. Circular dichroism (CD) typically expresses the chiral response. The structure has excellent absorption of right circularly polarized light while reflecting left circularly polarized light, and it is theoretically analyzed using the Jones matrix. By incorporating graphene between the gold hole array and the dielectric, the CD can be finely tuned. The CD response decreases from 0.88 to 0.55 when the Fermi energy level of graphene is changed from 0.3 eV to 1.0 eV, as indicated by computational studies. In addition, the periodic cell structure based on this metasurface can realize the digital imaging function and the dynamic modulation of the imaging state can be achieved by adjusting the Fermi energy level, which has potential applications in fields like communication encryption.**

***Index Terms*—Chiral metasurface, circular dichroism, graphene.**

I. Introduction

CHIRALITY is a structural property of an object that cannot be overlapped by translation and rotation with its mirror structure [1], and there are numerous substances in nature with chirality which respond differently to different circularly polarized light, such as DNA, amino acids, glucose, and certain viral molecules. Circular dichroism (CD) can be used to characterize the strength of the chiral response, which is defined as the difference in the structure's absorbance between right-hand circularly polarized (RCP) and left-hand circularly polarized (LCP) waves [2], [3], [4], [5]. The CD in chiral molecular spectrum is commonly used to determine the concentration of glucose in foods [6], [7], and it is also an important tool for determining information about the secondary structure of proteins and their related properties [8]. However, the CD of natural chiral molecules is weak, which severely limits their practical applications in biomolecular detection and electromagnetic wave polarization modulation. Therefore, artificial chiral materials have advantages due to more intense CD response, and with the intensive research on electromagnetic metamaterials, people have started to utilize chiral metamaterials to improve the CD response [9], [10], [11].

Recently, many chiral metamaterials and chiral metasurface structures have been proposed, mostly achieving extremely intense CD response. For example, Jiang et al. used a cascaded Huygens surface constructed from a double-layer silicon rod array to achieve both efficient and broadband transmissive CD and reflective CD, laying the theoretical groundwork for the design of multifunctional polarization modulation devices [12]. Wu et al. proposed a rectangular array of holes distributed in a honeycomb arrangement to achieve a stronger CD by varying the rotation angle of the rectangular holes. They also explored some laws affecting the strength of the chiral response, thereby providing us with more novel design ideas for chiral structures [13]. However, these metamaterials all have the disadvantage of having a single operating state and non-tunable, so a large number of tunable metasurfaces have been developed and intensively investigated, and the tuning methods have been classified as temperature control [14], [15], electrical control [16], [17], and light control [18], [19]. Kashif et al. [15] designed an adjustable resonant structure based on VO_2 by utilizing the metal-insulator phase transition properties of VO_2. But the response time of the temperature-controlled metasurface may be too slow to satisfy the demand for high-speed micro-nano devices in real-world applications [20], [21]. Liu et al. elicited a robust CD response by manipulating the angle of light incidence, and the CD response of the structure can be modulated, but its modulation degree could be further improved [19]. Graphene is a two-dimensional material with dynamic control, and has been applied in the research of tunable metamaterials for its unique optoelectronic properties [22], [23], [24]. Based on previous studies, Jiang et al. incorporated graphene into the design of the metasurface and discovered that the wavelength of its response could be altered by tuning graphene. In addition, they also focused on investigating the tunable asymmetric transmission properties of the tunable metasurface and its sensing properties, and the modulation effect is very satisfactory [25]. Therefore, the present work also employs graphene as an intermediate material to modulate the chiral response results of the metasurface structure with the aim of tuning its spectral amplitude.

Manuscript received 31 July 2023; accepted 3 August 2023. Date of publication 7 August 2023; date of current version 21 August 2023. This work was supported in part by the National Natural Science Foundation of China under Grants 62165004 and 61805053, in part by Guangxi Natural Science Foundation under Grant 2023GXNSFAA026108, in part by Innovation Project of GUET Graduate Education under Grants 2022YCXS047 and 2021YCXS040, and in part by the National Key R&D Program of China under Grant 2019YFB2203302. *(Corresponding author: Hongyan Yang.)*

Gongli Xiao, Sitong Zhou, and Haiou Li are with the Guangxi Key Laboratory of Precision Navigation Technology and Application, Guilin University of Electronic Technology, Guilin 541004, China.

Hongyan Yang is with the Guangxi Key Laboratory of Optoelectronic Information Processing, School of Optoelectronic Engineering, Guilin University of Electronic Technology, Guilin 541004, China (e-mail: hyyang@guet.edu.cn).

Bing Wang is with the School of Electronics and Information Technology, Sun Yat-Sen University, Guangzhou 510006, China.

Digital Object Identifier 10.1109/JPHOT.2023.3303038

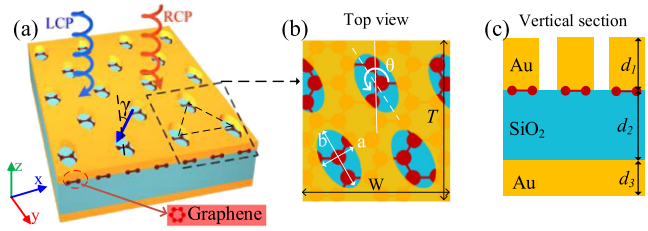

Fig. 1. (a) Schematic diagram of the elliptical hole array structure. (b) Top view of one periodic cell. (c) Vertical structural section.

In the present work, we propose a graphene-elliptic hole array composite structure, which can achieve tuning of the response strength of asymmetric transport properties by controlling the Fermi energy level of graphene. The effect of the elliptical rotation angle on the CD of the structure is firstly discussed. Next, we embed graphene between hole arrays and silica media to realize dynamic modulation of circular dichroism by tuning the Fermi energy levels. We also discuss the effect of the incidence angle of light on the absorption and CD of the structure, which has a robust absorption capacity for RCP between -14 and 14 degrees of incidence angle. In addition, as the period (T) in the y-direction of the structure varies, the corresponding response wavelength varies regularly with T. The array unit composed of this metasurface structure has some application value for dynamic image encryption.

II. Structure and Theory

The periodic structure of the elliptical hole array is shown in Fig. 1(a), which consists of three triangularly distributed elliptical holes forming a periodic cell. A top view of a periodic cell is shown in Fig. 1(b), with the length $W = 30$ μm in the x-direction and the length in the y-direction which we define as the periodic variable (T). The size of the short axis of the elliptical hole is a $= 7$ μm, the size of the long axis is b $= 12$ μm, and the angle of rotation of the elliptical hole counterclockwise is θ. The vertical section is shown in Fig. 1(c), and the materials of the structure from top to bottom are Au, SiO_2, and Au, respectively, and the thicknesses are $d_1 = 12$ μm, $d_2 = 15$ μm, the size of d_3 only needs to satisfy the role of the bottom metal reflector. The permittivity of Au was taken from Olmon et al. [26] and the refractive index of SiO_2 was taken from Popova et al. [27].

Firstly, we have to import the required material data in the software and then build the structure as shown in Fig. 1(a). The graphene used here is a single layer graphene with a thickness of 0.34 nm, and the ambient temperature is 300 K during the simulation. After that, we add the simulation region, set the boundary conditions in the x and y directions as aperiodic, the z direction as PML, and the mesh accuracy as 2. After that, we can add high precision mesh according to the specific needs of the simulation. There is no circular polarization source in FDTD, so we need to set it manually as follows: add two sources at the same time, first setting the polarization angle and phase of source1 to 0° and 0°. When defining the LCP light, set the polarization angle and phase of source2 to 90° and 90°; when defining the RCP light, set the polarization angle and phase of source2 to 90° and −90°, the reader can set a line monitor below the light source to check the light source. After the structure is all built, material fitting is performed, and successful fitting is followed by simulation verification.

Related experimental processes have been reported, we can manufacture it by the experimental process as follows. Firstly, we can grow a gold film on the substrate by evaporation method of vacuum coating [28], and cover the gold film with silicon dioxide (SiO_2) by the sol-gel process [29]. Then, monolayer graphene is grown on copper foil by chemical vapor deposition (CVD) and then transferred to SiO_2 by a transfer technique [30]. Next, the ionic gel solution was uniformly spin coated on the surface of graphene using a spin coater, and a uniform ionic gel film was formed on the surface of graphene, another strip electrode was fabricated on the upper surface of the ionic gel using Ag gel [31]. Finally, we can cover the anodic aluminum oxide (AAO) template on SiO_2, and after sputtering, separate the template to form the top array of gold holes [32].

We assume that the circularly polarized wave (CP) is incident along the negative direction of the z-axis, the incident field can be expressed as:

$$E_i(r,t) = \begin{pmatrix} i_x \\ i_y \end{pmatrix} \cdot e^{i(kz-\omega t)}, \tag{1}$$

where ω denotes the angular frequency of the incident light, k denotes the wave vector, and i_x and i_y denote the polarization state of the incident light. The reflected field of this incident light after passing through the chiral structure array can be expressed as:

$$E_R(r,t) = \begin{pmatrix} R_x \\ R_y \end{pmatrix} \cdot e^{i(kz-\omega t)}, \tag{2}$$

The relationship between the incident and reflected waves can be described by the Jones matrix [33], [34], [35]:

$$\begin{pmatrix} R_x \\ R_y \end{pmatrix} = \begin{pmatrix} R_{xx} & R_{xy} \\ R_{yx} & R_{yy} \end{pmatrix} \begin{bmatrix} i_x \\ i_y \end{bmatrix}, \tag{3}$$

The Jones matrix is expressed as $R_{IN} = \begin{pmatrix} R_{xx} & R_{xy} \\ R_{yx} & R_{yy} \end{pmatrix}$, If the structure has mirror asymmetry, then $R_{xy} \neq R_{yx}$. The transformation matrix Λ is usually used to transform the Jones matrix in the linearly polarized basis into the Jones matrix in the circularly polarized basis, and the transformation equation is as follow [36], [37]:

$$R_{circular} = \Lambda^{-1} R_{linear} \Lambda, \tag{4}$$

where $\Lambda = \frac{1}{\sqrt{2}} \begin{bmatrix} 1 & 1 \\ i & -i \end{bmatrix}$, and the transformed circularly polarized Jones matrix can be expressed as:

$$R_{cir} = \begin{bmatrix} R_{++} & R_{+-} \\ R_{-+} & R_{--} \end{bmatrix} = \frac{1}{2} \times \begin{pmatrix} [R_{xx}+R_{yy}+i(R_{xy}-R_{yx})] & [R_{xx}-R_{yy}-i(R_{xy}+R_{yx})] \\ [R_{xx}-R_{yy}+i(R_{xy}+R_{yx})] & [R_{xx}+R_{yy}-i(R_{xy}-R_{yx})] \end{pmatrix}, \tag{5}$$

The elements of the primary diagonal represent the reflection coefficients of isotropic circular polarization states (RCP

incidence - RCP reflection, LCP incidence - LCP reflection); the elements of the secondary diagonal represent the reflection coefficients of crossed circular polarization states (LCP incidence - RCP reflection, RCP incidence - LCP reflection). Combining the above equations, it can be seen that when the left circularly polarized wave and the right circularly polarized wave are simultaneously incidents on the chiral structure of this design, the structure will have a strong circular dichroism (CD) because its symmetry is broken, and then the main diagonal element exists $R_{++} \neq R_{--}$.

Graphene is a dynamically tunable two-dimensional material well in the mid-infrared and terahertz bands, and its conductivity equation can be expressed by the Kubo formula [38], [39]:

$$\sigma(\omega) = i\frac{e^2 E_f}{\pi\hbar^2(\omega + i/\tau)} - i\frac{e^2}{4\pi\hbar^2}\ln\left[\frac{2E_f + \hbar(\omega + i/\tau)}{2E_f - \hbar(\omega + i/\tau)}\right], \tag{6}$$

Where $\hbar = h/2\pi$, h denotes the Planck constant, E_f, ω and τ denote the Fermi energy level, the angular frequency, and the carrier relaxation time, respectively. $\tau = \mu E_f / e\nu_f^2$, μ and ν_f denote the carrier mobility and Fermi velocity, respectively. The working electromagnetic wave is in the mid-infrared band, satisfying $h\omega \leq 2E_f$, the conductivity of graphene is dominated by the intraband response, and the interband response is very weak and can be neglected, then the conductivity can be simplified as $\sigma(\omega) = i\frac{e^2 E_f}{\pi\hbar^2(\omega + i/\tau)}$. And the relationship between relative permittivity and conductivity of graphene can be expressed by the following equation [22]:

$$\varepsilon_r = 1 + {}^{i\sigma}/_{\omega\varepsilon_0 N_g t}, \tag{7}$$

where ε_r is the relative permittivity, ε_0 is the permittivity of free space, and t is the thickness of the graphene layer. $\varepsilon = \varepsilon_r \cdot \varepsilon_0$, where ε is permittivity.

III. Results and Analysis

We simulated the structure of the unembedded graphene layer with FDTD, setting $\theta = 22°$ and $T = 15$ μm, and analyzed the results. From Fig. 2(a), it can be observed that there is a huge difference in the absorption of LCP and RCP by the structure, and the surface electric field responses of LCP and RCP are completely different, which is probably the reason for the huge difference in absorption. And the resulting CD can be as high as 0.91, as shown in the blue line in Fig. 2(a). In addition, we found that the CD spectrum has an extremely narrow full width at half maxima (FWHM) of only 17 nm, and this means the CD spectrum with a high Q-factor, which is valuable in high-resolution imaging and high-sensitivity chiral sensing. This may be due to the generation of quadrupole resonance in the elliptical hole under RCP as shown in the electric field diagram in Fig. 2(a), and the breakdown of structural symmetry leads to further excitation of the Fano resonance by the resonant mode interacting with the RCP light, Fano resonance and the extraordinary optical transmission (EOT) of the holes array result in a reflection spectrum with extremely narrow linewidth [40].

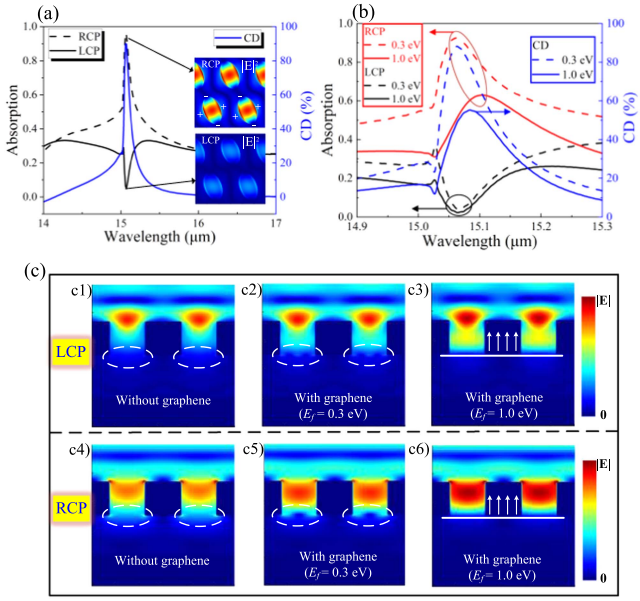

Fig. 2. (a) Absorption spectra of the structure for LCP and RCP without embedded graphene layer. (b) Absorption spectra of structures at different Fermi energy levels for LCP and RCP. (c1), (c4) the electric field responses under LCP and RCP without embedded graphene layers, respectively, (c2), (c5) the electric field response at LCP and RCP at $E_f = 0.3$ eV, respectively, (c3), (c6) the electric field response at LCP and RCP at $E_f = 1.0$ eV, respectively.

A graphene layer is sandwiched between the SiO_2 and Au layers. The structure is simulated while maintaining the structural parameters. As depicted in Fig. 2(b), when the Fermi energy level is 0.3 eV, the structure still generates a significant difference in the absorption of LCP and RCP at wavelengths slightly greater than 15 μm. We tune the Fermi energy level of graphene from 0.3 eV to 1.0 eV, and there is a very large decrease in the absorption of the structure to RCP, as depicted by the red line in Fig. 2(b), from 0.93 to 0.62, while the amplitude of absorption of LCP changed very little. As a result, CD decreases from 0.88 to 0.55, as depicted by the blue line in Fig. 2(b), indicating that the CD response of the structure can be tuned by altering the Fermi energy level by adjusting the external bias of graphene.

To further comprehend the physical mechanism of chiral tuning, the electric field response of LCP and RCP at various Fermi energy levels is plotted in Fig. 2(c). When the graphene layer is not embedded, as depicted in Fig. 2(c1), a large electric field converges at the top of the hole under the LCP wave, preventing energy from passing through the structure. There is essentially no interaction between the structure and the LCP wave, and there is no energy loss, so the structure reflects LCP waves strongly. And as depicted in Fig. 2(c4), the RCP wave interacts with the gold surface and generates the surface plasmon resonance (SPR) phenomenon [41], [42], in which the electrons on the gold surface absorb the energy of the photons. A portion of the energy can also enter the gold hole and travel downward, resulting in SPR at the interface between the bottom of the hole and the dielectric's surface. This energy depletion significantly reduces the intensity of the reflected wave, making it highly absorbent under the RCP.

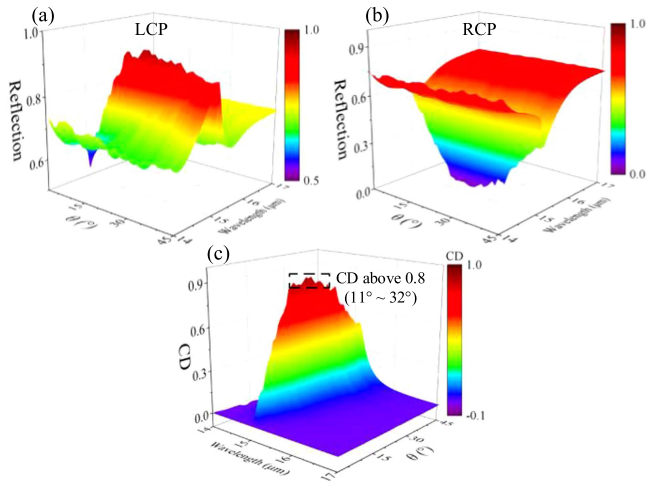

Fig. 3. Results of parametric scan of θ from 0∼45°, (a) reflection spectrum of LCP wave, (b) reflection spectrum of RCP wave, (c) CD spectrum.

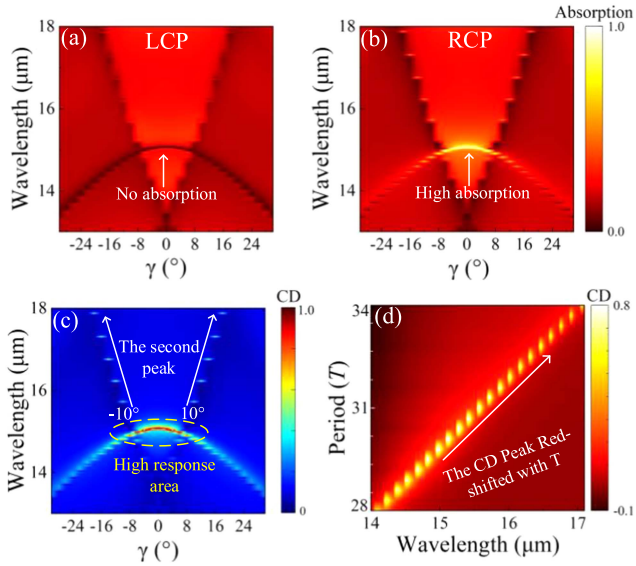

Fig. 4. (a) Absorption evolution at LCP, (b) absorption evolution at RCP. (c) CD spectrum evolution at −30∼30° incidence. (d) Evolution of the CD spectrum peak at different T.

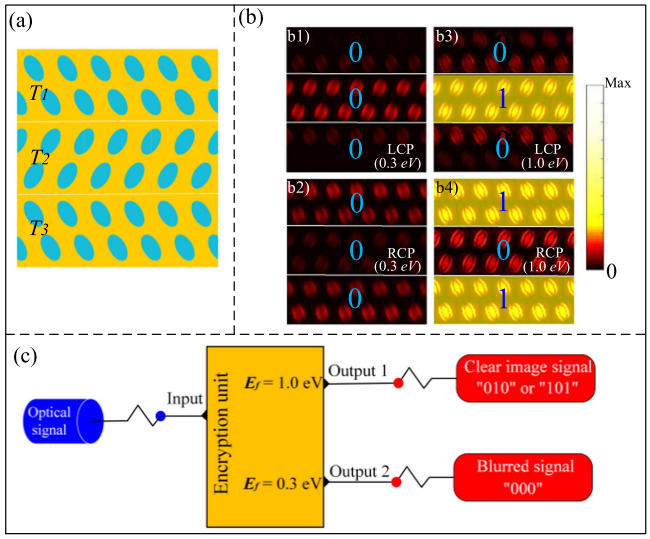

Fig. 5. (a) Digital imaging unit. (b) The electric field distribution at the Fermi energy level of 0.3 eV or 1.0 eV, (b1) LCP waves incident, $E_f = 0.3$ eV. (b2) RCP waves incident, $E_f = 0.3$ eV. (b3) LCP waves incident, $E_f = 1.0$ eV. (b4) RCP waves incident, $E_f = 1.0$ eV. (c) Imaging encryption mechanism.

Next, we also show the results of the electric field response after embedding the graphene layer. As shown in (6), the conductivity of graphene increases with the increasing of E_f, and as shown in (7), the permittivity is directly proportional to the change of conductivity, when E_f is very low, its dielectric constant is small and its responsiveness to the electric field is weak, so the electric field can easily penetrate the graphene. And as E_f gradually gets higher, its binding force to the electric field becomes stronger and it is not easy to be penetrated by the electric field, which is equivalent to a metal reflective layer. Thus, the E_f change from 0.3 eV to 1.0 eV can be interpreted as a transition of graphene from dielectric properties to metallic properties [43]. As shown in Fig. 2(c2) and (c5), graphene is in a dielectric state at this point and is easily penetrated by the electric field, hence there is little change compared to the results without embedded graphene. As shown in Fig. 2(c3) and (c6), the graphene is metal properties at this point. While the top of the gold still interacts with the RCP wave to generate SPR, the energy entering the hole cannot pass through the graphene layer and is partially reflected back, and the SPR is no longer generated between the dielectric and the bottom of the gold, so the absorption of RCP by the structure decreases more substantially.

We also investigate the effect of the elliptical hole's rotation angle (θ) on the structural CD's strength. The angle is scanned in 1° increments from 0 to 45 degrees, and the results are analyzed. Fig. 3(a) and (b) illustrate the effect of θ on the structure's reflection coefficient under LCP and RCP, respectively. And it can be seen in Fig. 3(c) that θ is between 11° and 32°, the structures can all achieve a strong CD above 0.8, and the CD begins to decrease swiftly above 36°, indicating that angle size plays a crucial role in the chirality of the structures.

Here, we investigated the effect of the incident angle γ on the absorption and CD of the structure. Fig. 4(a) and (b) show the absorption of LCP and RCP waves at incidence angles from −30° to 30°. The results show that the structure has good wide-angle absorption for RCP in the incidence range of −14° to 14°, but does not have absorption properties for either LCP. A strong CD of more than 0.7 can be maintained at an incidence angle of −9° to 9° is as shown in Fig. 4(b). In addition, we also find that a stronger CD peak is again generated at the points above −10° and 10° of γ, as shown by the white arrow in Fig. 4(c), the CD peak is redshifted as γ becomes larger. Perhaps the change in the angle of incidence breaks the symmetry of the structure again, leading to a double breakage in structural symmetry, and resulting in two peaks in the CD spectrum. Furthermore, we also try to explore how the y-directional period T of the structure affects the results. Fig. 4(d) shows that different response wavelengths (λ) correspond to different T, and it can be

directly observed that the relationship between T and λ roughly satisfies $\lambda = T/2$. Therefore, this result shows that we can tune the response wavelength of the structure by changing the period parameter T.

Based on the preceding analysis, we can comprehend the fundamental mechanism of the chiral metamaterial structure, which can absorb RCP and reflect LCP and whose CD can be dynamically adjusted by altering the Fermi energy level of graphene to a certain degree. Consequently, in Fig. 5(a), we illustrate a periodic structure with a 3×3 arrangement and demonstrate the application of this chiral metasurface for near-field imaging encryption by exploiting the unit structure of its periodic units. Here, we denote the weak field response of the near-field distribution as "0" and the strong electric field response as "1". When $E_f = 0.3$ eV, we find that the signal output result is "000" for both LCP and RCP waves, as shown in Fig. 5(b1) and (b2). When $E_f = 1.0$ eV, the digital signals under the LCP and RCP waves are "010" and "101", respectively, as shown in Fig. 5(b3) and (b4). These show that it is possible to interfere with the clear imaging signal through external dynamic modulation and thus encrypt them. In Fig. 5(c), the working mechanism of imaging encryption is visually demonstrated. In addition, this chiral metasurface are expected to enable tunable half-wave plates or quarter-wave plates by controlling the direction of rotation of the elliptical hole.

IV. Conclusion

In summary, based on theoretical analysis of the model, this study proposes a graphene-Au elliptical holes array metasurface structure. The CD response is significantly affected by the rotation angle of elliptical holes and the incidence angle of light, according to an analysis of the data. Then, we incorporated graphene layers and demonstrated that the CD response can be dynamically tailored by altering its Fermi energy level. Moreover, a correlation between response frequency and period was discovered. Finally, we arrayed a 3×3 arrangement of cells to implement near-field digital imaging, and the results have important applications in imaging encryption and communication.

References

[1] V. Fedotov, P. Mladyonov, S. Prosvirnin, A. Rogacheva, Y. Chen, and N. Zheludev, "Asymmetric propagation of electromagnetic waves through a planar chiral structure," *Phys. Rev. Lett.*, vol. 97, no. 16, 2006, Art. no. 167401.

[2] R. W. Woody, "[4] Circular dichroism," in *Biochemical Spectroscopy* (Methods in Enzymology), vol. 246. Amsterdam, The Netherlands: Elsevier, 1995, pp. 34–71.

[3] N. Berova, K. Nakanishi, and R. W. Woody, *Circular Dichroism: Principles and Applications*. Hoboken, NJ, USA: Wiley, 2000.

[4] Z. Wang, H. Jia, K. Yao, W. Cai, H. Chen, and Y. Liu, "Circular dichroism metamirrors with near-perfect extinction," *Amer. Chem. Soc. Photon.*, vol. 3, no. 11, pp. 2096–2101, 2016.

[5] P. Wu et al., "Non-uniform self-folding of helical poly (fluorenevinylene) derivatives in the solid state leading to amplified circular dichroism and circularly polarized light emission," *Angewandte Chemie Int. Ed.*, vol. 61, no. 43, 2022, Art. no. e202210556.

[6] F. Cunha, R. de Holanda, A. Secchi, M. de Souza Jr, and A. Barreto Jr, "Simultaneous absorption of UV-vis and circular dichroism to measure enantiomeric concentrations of praziquantel under nonlinear conditions," *Spectrochimica Acta Part A: Mol. Biomol. Spectrosc.*, vol. 241, 2020, Art. no. 118645.

[7] K. Ngamdee and W. Ngeontae, "Circular dichroism glucose biosensor based on chiral cadmium sulfide quantum dots," *Sensors Actuators B: Chem.*, vol. 274, pp. 402–411, 2018.

[8] S. E. Spencer and A. Rodger, "Bayesian inference assessment of protein secondary structure analysis using circular dichroism data-how much structural information is contained in protein circular dichroism spectra?," *Anal. Methods*, vol. 13, no. 3, pp. 359–368, 2021.

[9] Z. Shen, X. Fang, S. Li, L. Zhang, and X. Chen, "Mechanically reconfigurable and electrically tunable active terahertz chiral metamaterials," *Extreme Mechanics Lett.*, vol. 51, 2022, Art. no. 101562.

[10] S. Han, H. Yang, L. Guo, X. Huang, and B. Xiao, "Manipulating linearly polarized electromagnetic waves using the asymmetric transmission effect of planar chiral metamaterials," *J. Opt.*, vol. 16, no. 3, 2014, Art. no. 035105.

[11] C. Huang, J. Zhang, Q. Cheng, and T. Cui, "Multi-band tunable asymmetric transmission of linearly polarized electromagnetic waves achieved by active chiral metamaterial," in *Proc. Photon. Electromagn. Res. Symp.-Fall*, 2019, pp. 325–331.

[12] H. Jiang, W. Zhao, and Y. Jiang, "All-dielectric circular polarizer with nearly unit transmission efficiency based on cascaded tensor Huygens surface," *Opt Exp.*, vol. 24, no. 16, pp. 17738–17745, Aug. 2016, doi: 10.1364/OE.24.017738.

[13] B. Wu et al., "Near-infrared chirality of plasmonic metasurfaces with gold rectangular holes," *Adv. Composites Hybrid Mater.*, vol. 5, no. 3, pp. 2527–2535, 2022, doi: 10.1007/s42114-022-00513-3.

[14] M. Liu et al., "Temperature-controlled optical activity and negative refractive index," *Adv. Funct. Mater.*, vol. 31, no. 14, 2021, Art. no. 2010249.

[15] M. F. Kashif et al., "Design of vanadium-dioxide-based resonant structures for tunable optical response," *Opt. Lett.*, vol. 47, no. 9, pp. 2286–2289, May 2022, doi: 10.1364/OL.455457.

[16] R. Zhang, B. You, S. Wang, K. Han, X. Shen, and W. Wang, "Broadband and switchable terahertz polarization converter based on graphene metasurfaces," *Opt. Exp.*, vol. 29, no. 16, pp. 24804–24815, 2021.

[17] J. Zhu, S. Li, L. Deng, C. Zhang, Y. Yang, and H. Zhu, "Broadband tunable terahertz polarization converter based on a sinusoidally-slotted graphene metamaterial," *Opt. Mater. Exp.*, vol. 8, no. 5, pp. 1164–1173, 2018.

[18] S. Zhou et al., "Tunable chiroptical response of graphene achiral metamaterials in mid-infrared regime," *Opt. Exp.*, vol. 27, no. 11, pp. 15359–15367, 2019.

[19] C. Liu et al., "Giant asymmetric transmission and circular dichroism with angular tunability in chiral terahertz metamaterials," *Annalen Der Physik*, vol. 532, no. 3, 2020, Art. no. 1900398, doi: 10.1002/andp.201900398.

[20] X. Zhao et al., "Multifield controlled terahertz modulator based on silicon-vanadium dioxide hybrid metasurface," *Adv. Opt. Mater.*, vol. 10, no. 10, 2022, Art. no. 2102589.

[21] K. M. Devi, A. Jana, S. Rane, P. R. Choudhury, and D. R. Chowdhury, "Temperature tunable electromagnetically induced transparency in terahertz metasurface fabricated on ferroelectric platform," *J. Phys. D: Appl. Phys.*, vol. 55, no. 49, 2022, Art. no. 495103.

[22] L. A. Falkovsky, "Optical properties of graphene," *J. Phys.: Conf. Ser.*, vol. 129, 2008, Art. no. 012004, doi: 10.1088/1742-6596/129/1/012004.

[23] F. Li et al., "Metal-graphene hybrid chiral metamaterials for tunable circular dichroism," *Annalen Der Physik*, vol. 532, no. 7, 2020, Art. no. 2000065, doi: 10.1002/andp.202000065.

[24] N. Huo et al., "Interlayer coupling and optoelectronic properties of ultrathin two-dimensional heterostructures based on graphene, MoS 2 and WS 2," *J. Mater. Chem. C*, vol. 3, no. 21, pp. 5467–5473, 2015.

[25] H. Jiang, W. Zhao, and Y. Jiang, "High-efficiency tunable circular asymmetric transmission using dielectric metasurface integrated with graphene sheet," *Opt. Exp.*, vol. 25, no. 17, pp. 19732–19739, Aug. 2017, doi: 10.1364/OE.25.019732.

[26] R. L. Olmon et al., "Optical dielectric function of gold," *Phys. Rev. B*, vol. 86, no. 23, 2012, Art. no. 235147.

[27] S. Popova, T. Tolstykh, and V. Vorobev, "Optical characteristics of amorphous quartz in the 1400-200 cm−1 region," *Opt. Spectrosc*, vol. 33, pp. 444–445, 1972.

[28] R. Zahra et al., "Effect of secondary phases on the thermoelectric properties of Zn_2GeO_4 nano-crystals grown by thermal evaporation on Au coated Si substrate," *Physica B: Condens. Matter*, vol. 564, pp. 143–146, 2019.

[29] S. Ogawa, A. S. Idris, Y. Han, H. Jiang, and K. Hamamoto, "Surface improvement investigation of sol-gel SiO2 cladding for waveguide device passivation," *Japanese J. Appl. Phys.*, vol. 58, no. SJ, 2019, Art. no. SJJB04.

[30] Y. Cheng, K. Wang, Y. Qi, and Z. Liu, "Chemical vapor deposition method for graphene fiber materials," *Acta Physico-Chimica Sinica*, vol. 38, no. 2, 2022, Art. no. 2006046.

[31] Y. Yinghui, C. Xieyu, H. Fangrong, X. Xianming, Z. Wentao, and H. Jiaguang, "Terahertz amplitude modulator based on metasurface/ion-gel/graphene hybrid structure," *Chin. J. Lasers*, vol. 46, no. 6, 2019, Art. no. 0614016.

[32] S. Liu, J. Tian, and W. Zhang, "Fabrication and application of nanoporous anodic aluminum oxide: A review," *Nanotechnology*, vol. 32, no. 22, Mar. 2021, Art. no. 222001, doi: 10.1088/1361-6528/abe25f.

[33] N. K. Grady et al., "Terahertz metamaterials for linear polarization conversion and anomalous refraction," *Science*, vol. 340, no. 6138, pp. 1304–1307, 2013.

[34] C. Pfeiffer, C. Zhang, V. Ray, L. J. Guo, and A. Grbic, "High performance bianisotropic metasurfaces: Asymmetric transmission of light," *Phys. Rev. Lett.*, vol. 113, no. 2, 2014, Art. no. 023902.

[35] T. Xu and H. J. Lezec, "Visible-frequency asymmetric transmission devices incorporating a hyperbolic metamaterial," *Nature Commun.*, vol. 5, no. 1, pp. 1–7, 2014.

[36] H. Li et al., "Diatomic terahertz metasurfaces for arbitrary-to-circular polarization conversion," *Nanoscale*, vol. 14, no. 35, pp. 12856–12865, Sep. 2022, doi: 10.1039/d2nr03483b.

[37] E. Plum, V. A. Fedotov, and N. I. Zheludev, "Extrinsic electromagnetic chirality in metamaterials," *J. Opt. A: Pure Appl. Opt.*, vol. 11, no. 7, 2009, Art. no. 074009, doi: 10.1088/1464-4258/11/7/074009.

[38] H.-J. Li et al., "Graphene-based mid-infrared, tunable, electrically controlled plasmonic filter," *Appl. Phys. Exp.*, vol. 7, no. 2, 2014, Art. no. 024301.

[39] X. He, "Tunable terahertz graphene metamaterials," *Carbon*, vol. 82, pp. 229–237, 2015.

[40] Y. D. Shah, J. Grant, D. Hao, M. Kenney, V. Pusino, and D. R. S. Cumming, "Ultra-narrow line width polarization-insensitive filter using a symmetry-breaking selective plasmonic metasurface," *Amer. Chem. Soc. Photon.*, vol. 5, no. 2, pp. 663–669, 2017, doi: 10.1021/acsphotonics.7b01011.

[41] A. V. Zayats, I. I. Smolyaninov, and A. A. Maradudin, "Nano-optics of surface plasmon polaritons," *Phys. Rep.*, vol. 408, no. 3/4, pp. 131–314, 2005.

[42] I. P. Radko, S. I. Bozhevolnyi, G. Brucoli, L. Martín-Moreno, F. García-Vidal, and A. Boltasseva, "Efficiency of local surface plasmon polariton excitation on ridges," *Phys. Rev. B*, vol. 78, no. 11, 2008, Art. no. 115115.

[43] F. Li, T. Tang, Y. Mao, L. Luo, and J. Yao, "Metal-graphene hybrid chiral metamaterials for tunable circular dichroism," *Annalen Der Physik*, vol. 532, 2020, Art. no. 2000065.